J. N. E. Carneiro
Joao.Carneiro@sintef.no
Instituto SINTEF do Brasil
Rua Lauro Müller, 116/2201
22290-160 Rio de Janeiro, RJ, Brazil

R. Fonseca Jr.
robertofonseca@petrobras.com.br
CENPES, Petrobras
Rio de Janeiro, RJ, Brazil

A. J. Ortega
arturo.ortega@ntnu.no

R. C. Chucuya
roberto_chucuya@yahoo.es

A. O. Nieckele
nieckele@puc-rio.br

L. F. A. Azevedo
Lfaa@puc-rio.br
PUC-Rio
Department of Mechanical Engineering
22453-900 Rio de Janeiro, RJ, Brazil

Statistical Characterization of Two-Phase Slug Flow in a Horizontal Pipe

The present paper reports the results of an ongoing project aimed at providing statistical information on slugs in two-phase flow in a horizontal pipe. To this end, the flow was examined experimentally and numerically. On the experimental side, three non-intrusive optical techniques were combined and employed to determine the velocity field and bubble shape: particle image velocimetry (PIV), Pulsed Shadow Technique (PST) and Laser-Induced Fluorescence technique (LIF). Statistical information was provided by photogate cells installed at two axial positions. The flow was numerically determined based on the one-dimensional Two-Fluid Model. The tests were conducted on a specially built transparent pipe test section, using air and water as the working fluids. The velocity fields were obtained for flow regimes where the slugs were slightly aerated to facilitate the utilization of the optical methods employed. The main parameters for characterizing the statistically steady flow regime such as slug length and velocity obtained numerically were compared with the experimental data and good agreement was obtained.
Keywords: *slug-flow, horizontal pipe, numerical simulation, optical techniques*

Introduction

Intermittent two phase flow pattern, which is commonly defined as plug or slug flow, is frequently encountered in industrial applications. Relevant examples are found in oil/gas production and transport lines and in boiler and heat exchanger tubes for energy production plants. Classical flow maps (e.g., Mandhane et al., 1974), indicate that the intermittent slug and plug (or elongated bubble) flow regimes exist for a wide range of gas and liquid flow rates in a horizontal two-phase flow configuration.

Due to its intrinsic transient nature, slug flows can cause severe problems in processing and transport equipment due to the intermittent loading that it imposes on the structures. Also in hydrocarbon production lines, where the fluids transported may contain corrosive agents, slug flow is found to present safety risks due to damage imposed on pipe walls. According to Kvernvold et al. (1984), it is believed that the large fluctuations on the wall shear stress imposed by this flow pattern may remove protective corrosion products from the pipe wall facilitating the corrosive-erosive attacks. Due to its importance, a continuous research effort has been made to predict this complex flow pattern.

Nomenclature

A = *cross sectional area, m^2*
C_o = *distribution parameter*
D = *pipe diameter, m*
D_h = *hydraulic diameter, m*
f = *friction factor*
Fr = *Froude number*
g = *gravity acceleration, m/s)*
h_L = *liquid height, m*
L_s = *slug length, m*
p = *pressure, Pa*
R_G = *gas constant, [J/(kg K)]*
Re = *Reynolds number*
S = *wetted perimeter, m*
t = *time, s*
U = *velocity, m/s*
U_d = *drift velocity, m/s*
U_T = *translational slug velocity, m/s*
x = *axial coordinate, m*

Greek Symbols

α_G = *void fraction*
α_L = *liquid holdup*
β = *pipe inclination angle*
μ = *dynamic viscosity, Pa s*
υ = *frequency, s^{-1}*
ρ = *density, kg/m^3*
τ = *shear stress, Pa*

Subscripts

G = *gas*
i = *interface*
L = *liquid*
M = *mean*
s = *superficial*
S = *slug*
w = *wall*

The intermittent flow can originate from stratified gas-liquid flow when interface waves grow via a classical Kelvin-Helmotz instability to occupy the entire pipe cross section (Taitel and Duker, 1976), or/and by the accumulation of liquid at valleys of irregular terrains (Al Safran et al., 2005). Wave coalescence has also been observed as an important mechanism in the slug formation, especially at high gas flow rates in horizontal pipes (Woods et al., 2006; Sanchis et al., 2011).

The most significant parameters to characterize a slug flow are the gas and liquid phases' distribution, the liquid velocity and its fluctuation, the bubble frequency (or slug length) and the turbulent characteristics of mass, momentum and energy transfer at the interface (Sharma et al., 1998). Due to the intermittent and irregular character of the flow, these parameters present time variations. The knowledge of time averaged values of these quantities is not always sufficient for

design purposes, and statistical information might be relevant. For instance, the design of slug catchers has to be based on the longest possible slug, and not on the average one. According to Fabre and Liné (1992), the average slug length in horizontal pipe varies from 15 to 40 diameters, independently of the fluid properties and inlet velocities. Barnea and Taitel (1993) mentioned that the slug length distribution can present a large variance in relation to the mean value.

Several numerical and experimental works can be found in the literature aiming at analyzing the statistical variables related to the slug pattern (Cook and Behnia, 2000; Issa and Kempf, 2003; Want et al., 2007; Fonseca Jr. et al., 2009). Empirical observations and correlations of the main slug properties are extremely important to close models and to validate numerical results.

The present paper presents a numerical simulation of slug flow of air and water through a horizontal pipe employing the Two Fluid Model. An experimental program was conducted in parallel with the objective of providing statistical data on the slug properties to validate the numerical predictions. These properties encompassed slug frequency, length and translational velocity for a statistically steady regime. Also, the experimental test program was designed to allow the measurement of instantaneous information on the flow field and bubble shape in the plug and slug flow regimes. To this end, three non-intrusive, optical-based techniques were combined to yield the desired instantaneous flow field information.

Mathematical Modeling

The Two-Fluid Model consists of a set of conservation equations for each phase (Ishii and Hibiki, 2006). In the present work, a one dimensional formulation was employed, and the model equations were obtained through an average process in the flow cross-section. The flow was considered isothermal along a horizontal pipe, without mass transfer between the phases.

The liquid phase was modeled as incompressible, while the gas phase was governed by the ideal gas law:

$$\rho_G = p/(R_G\, T). \tag{1}$$

Based on previous studies (Carneiro et al., 2005; Carneiro and Nieckele, 2008), equality of pressure at both sides of the interface was also considered, and, for simplicity, the gas pressure was considered equal to its interfacial value.

The sum of each phase volume fraction must respect the following restriction,

$$\alpha_G + \alpha_L = 1. \tag{2}$$

The conservation equations of each phase are:

Continuity:

$$\frac{\partial(\rho_G\,\alpha_G)}{\partial t} + \frac{\partial(\rho_G\,\alpha_G U_G)}{\partial x} = 0 \tag{3}$$

$$\frac{\partial(\rho_L\,\alpha_L)}{\partial t} + \frac{\partial(\rho_L\,\alpha_L U_L)}{\partial x} = 0 \tag{4}$$

Linear momentum:

$$\frac{\partial(\rho_G\,\alpha_G U_G)}{\partial t} + \frac{\partial(\rho_G\,\alpha_G U_G^2)}{\partial x} = -\alpha_G \frac{\partial p}{\partial x} - \alpha_G\,\rho_G\, g \frac{\partial h_L}{\partial x}\mathbf{cos}\beta - \alpha_G\,\rho_G\, g\,\mathbf{sin}\beta - \frac{\tau_{wG}\,S_G}{A} - \frac{\tau_i\,S_i}{A} \tag{5}$$

$$\frac{\partial(\rho_L\,\alpha_L U_L)}{\partial t} + \frac{\partial(\rho_L\,\alpha_L U_L^2)}{\partial x} = -\alpha_L \frac{\partial p}{\partial x} - \alpha_L\,\rho_L\, g \frac{\partial h_L}{\partial x}\mathbf{cos}\beta - \alpha_L\,\rho_L\, g\,\mathbf{sin}\beta - \frac{\tau_{wL}\,S_L}{A} + \frac{\tau_i\,S_i}{A} \tag{6}$$

The averaging process leads to additional terms such as τ_{wL}, τ_{wG} and τ_i, which represent the shear stress at the liquid-wall, gas-wall and interface, respectively. These terms require closure equations to be determined.

Closure equations

The shear stresses were determined considering the flow as locally fully developed, thus:

$$\tau_{wG} = \frac{f_G}{2}\,\rho_G\, U_G\,|U_G| \quad ; \quad \tau_{wL} = \frac{f_L}{2}\,\rho_L\, U_L\,|U_L| \tag{7}$$

$$\tau_i = \frac{f_i}{2}\,\rho_G\,(U_G - U_L)\,|U_G - U_L| \tag{8}$$

There are several correlations available in the literature to determine the friction factor *f*. In the present work, the correlations listed in Table 1 were employed following the recommendation of Issa and Kempf (2003).

Table 1. Friction factor correlations.

	Re_G, Re_L, $Re_i \le 2100$ (Laminar)	Re_G, Re_L, $Re_i > 2100$ (Turbulent)
f_L	$24/\mathbf{Re}_{sL}$	$0.0262(\alpha_l\,\mathbf{Re}_{sL})^{0.139}$
f_G	$16/\mathbf{Re}_G$	$0.046(\mathbf{Re}_G)^{-0.25}$
f_i	$16/\mathbf{Re}_G$	$0.046(\mathbf{Re}_i)^{-0.25}$

The equations presented in Table 1 depend on the Reynolds numbers $\mathbf{Re}_{sL}$, $\mathbf{Re}_G$ and $\mathbf{Re}_i$ defined as (Taitel and Dukler, 1976):

$$\mathbf{Re}_{sL} = \frac{\rho_L\,U_{sL}\,D}{\mu_L} \quad ; \quad \mathbf{Re}_G = \frac{\rho_G\,U_G\,D_{hG}}{\mu_G} \tag{9}$$

$$\mathbf{Re}_i = \frac{\rho_G\,|U_G - U_L|\,D_{hG}}{\mu_G} \quad ; \quad D_{hG} = \frac{4A_G}{(S_G + S_i)} \tag{10}$$

where the gas and interface Reynolds numbers are based on the gas hydraulic diameter, D_{hG}. Further, μ is the dynamic viscosity of the phase, D is the pipe diameter and U_{sL} is the liquid superficial velocity, defined as $U_{sL} = \alpha_L U_L$.

Experiments

Figure 1 schematically presents the test section constructed to conduct the experiments. A 24-mm-diameter, 10-meters-long Plexiglas pipe was mounted on a rigid steel frame that could be rotated around a pivot to produce inclination angles between 0 and $+10^o$ with the horizontal. However, in this work, only horizontal case results are presented. The pipe length-to-diameter ratio was 400, which should be sufficient for the formation of stable slugs. Water from a reservoir was pumped in closed circuit through the test pipe by a progressive cavity pump. A centrifugal blower provided compressed air for the test section. Calibrated rotameters were used to measure the water and air flow rates. Air and water were mixed at

a Y-junction positioned at the entrance of the Plexiglas pipe. After passing through the test pipe, the two-phase mixture returned to the reservoir where a tangential inlet aided the phase separation process. The continuous and dashed arrows in Fig. 1(a) indicate, respectively, the water and air flow paths in the test section.

The measuring section was located at 350 diameters from the pipe entrance. As can be seen schematically in Fig. 1(b), the measuring section was specially prepared to receive the components necessary for the implementation of the three optical techniques employed in the experiments, namely, PIV (*Particle Image Velocimetry)*, LIF (*Laser-Induced Fluorescence technique)* and PST (*Pulsed Shadow Technique*). As seen in Fig. 1(b), a rectangular acrylic box filled with water was installed around the tube in the measuring region to minimize light refraction effects and improve the quality of the registered images of the flow.

The PIV technique is now widely used for measuring instantaneous flow fields in extended regions in single phase flows. Briefly, in its two-dimensional version, the technique relies on the digital processing of consecutive images of seed particles previously distributed in the flow. A relatively high energy laser pulse of short duration is used to illuminate a planar region of the flow freezing the particle images. To this end, laser firing is synchronized with image captured by a digital camera. The displacement field of the particles is obtained by cross correlating the images' pairs (Raffel et al., 2007).

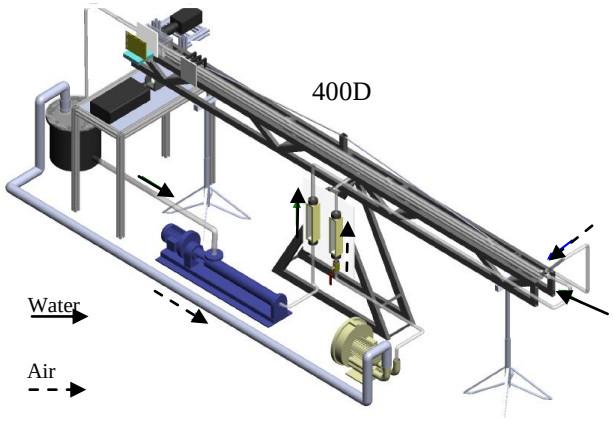

(a) Overview of test section.

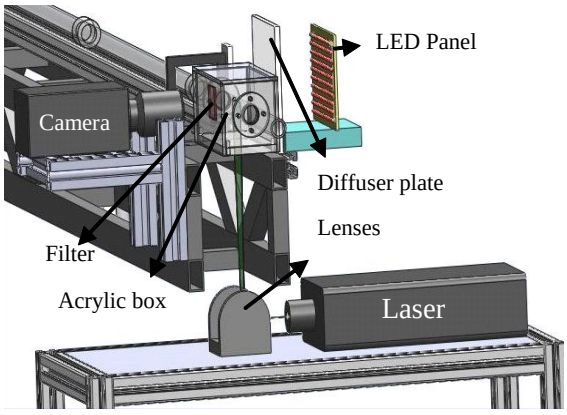

(b) Components of the measuring system.

Figure 1. Experimental apparatus.

The challenge for extending the PIV technique to gas-liquid flows resides on the elimination of intense light scattered by the liquid-gas interfaces that precludes the capture of the low intensity light scattered by the small tracer particles. The Laser Induced Fluorescence technique enables the registration of the tracer particle positions in gas-liquid flows. In this technique particles impregnated with fluorescent dye (Rhodamine B, in our experiments) were used as tracers. When illuminated by the green laser light, the fluorescent particles emit light in a wave length corresponding to red light. An optical filter chosen with an appropriate cut-off wave length blocks the intense green light scattered by the gas-liquid interface allowing the passage of the red light emitted by the tracer particles. A clear image of the tracer particles is then formed for each laser pulse, and can be cross correlated to yield the velocity field within the liquid phase of the gas-liquid flow.

In order to produce a sharp definition of the boundaries of the liquid and gas regions, the Pulsed Shadow Technique was employed together with the PIV and LIF techniques. A panel formed by a matrix of a 132 high energy red LEDs was assembled and mounted behind the test section, facing the digital camera, as indicated in Fig. 1(b). The LED panel was pulsed by a trigger signal synchronized to one of the laser firing signals. The red light emitted by LEDs was able to pass the optical filter and reach the camera sensor. The different attenuation of the LED light due to the passage through either the gas or liquid phases allowed a clear definition of the gas-liquid interfaces. More details of the optical techniques employed can be found in Fonseca Jr. et al. (2009).

Positioned just upstream of the visualization region there were two photocell sensors. These sensors were used to detect the passage of the gas or liquid phases. A low-to-high transition signal produced by the sensors as a result of the passage of a gas-liquid interface was registered by a data acquisition unit. The knowledge of the axial distance between the sensors allowed the determination of slug nose or tail velocity. The analysis of the signal produced by each individual sensor furnished the frequency and slug length data (Fonseca Jr. et al., 2009). After acquiring the data, lengths smaller than 3 diameters were considered as disperse bubbles and were discarded.

Numerical Method

The conservation equations were discretized with the finite volume method, which consists on integration of the conservation equations at each control volume. While all scalar variables were stored at the central nodal point, a staggered mesh was employed for the velocities. The convective terms were integrated with the upwind approximation, and the temporal integration was performed with the fully implicit Euler scheme. The void fraction is obtained from the gas mass conservation equation, while the gas and liquid velocities were obtained from the solution of their respective momentum equations. Pressure is determined indirectly from the global mass conservation equations, which can be obtained by combining the gas and liquid conservation equations. Issa and Kempf (2003) recommended to normalize each phase conservation equation based on the density before combining them, resulting in

$$\frac{1}{\rho_{G_{ref}}}\left[\frac{\partial(\rho_G \alpha_G)}{\partial t}+\frac{\partial(\rho_G \alpha_G U_G)}{\partial x}\right]+\left[\frac{\partial \alpha_L}{\partial t}+\frac{\partial(\alpha_L U_L)}{\partial x}\right]=0 \quad (11)$$

These equations were solved sequentially through an iterative method, which handles the velocity-pressure coupling based on the PRIME algorithm (Ortega and Nieckele, 2005). The solution of the algebraic system was performed with the TDMA algorithm.

Since the gas momentum equation becomes singular when the void fraction becomes zero, this equation was not solved when a slug was formed ($\alpha_g < 0.02$), and the gas velocity was arbitrarily set to zero, as recommended by Issa and Kempf (2003).

A grid test was performed and a mesh with 750 points was selected, for presenting differences inferior to 5%. The time step was defined such that the Courant number $C = u\Delta t/\Delta x$ was always inferior to 0.1.

Mean slug parameters

The velocity of each slug is obtained by measuring the time interval taken by the slug to travel between two previously defined numerical probes at two positions (x_1 and x_2). The distance between the probes was taken to be equal to 10*D*, based on a preliminary analysis, in which no difference in the results was observed by varying the probe distances from 5*D* to 15*D*. The timer was triggered when the gas volume fraction reached values inferior to 2% at the first probe position. The timer was turned off when the gas volume fraction reached values inferior to 2% at the second probe. Thus, the translational velocity of slug *k* can be obtained by

$$U_{T,k} = \frac{x_2 - x_1}{\Delta t_{1\to 2}} \tag{12}$$

The slug length is determined by continuously monitoring the gas volume fraction at probe position x_2, in order to identify the time instants that the nose and tail of a liquid slug reach that position. α_G values below 2% indicate the arrival of a slug, and triggers the timer, which is turned off when α_G values above 2% are measured, indicating that the tail is passing through the same probe x_2. The length of slug *k* at probe position x_2 can then be determined, considering that the previously obtained translation slug velocity was constant during this time interval, by

$$L_{S,k} = U_{T,k}\Delta t_{n\to t} \tag{13}$$

where *n* and *t* imply slug "nose" and "tail", respectively.

The average slug frequency (υ_s) is defined based on the number of slugs that pass through a certain position (x_o) during a time interval, as indicated by Eq. (14), and it is measured during the whole simulation.

$$\langle \upsilon_S \rangle = \frac{1}{N}\sum_{k=1}^{N}\frac{1}{\Delta t_k} \tag{14}$$

Average slug and bubble velocities and average slug lengths were computed as:

$$\langle U_T \rangle = \frac{1}{N}\sum_{k=1}^{N} U_{T,k}, \quad \langle U_B \rangle = \frac{1}{N}\sum_{k=1}^{N} U_{B,k}, \quad \langle L_S \rangle = \frac{1}{N}\sum_{k=1}^{N} L_{S,k}, \tag{15}$$

where *N* is the number of values computed from the solutions.

Results

The numerical solution was obtained for a pipe with the same diameter and length as the one employed in the experiments. The temperature was considered constant and equal to 298 K. The air gas constant and absolute viscosity were set as R_G = 287 N m/(kg K) and $\mu_G = 1.790 \times 10^{-5}$ Pa s. The water density and absolute viscosity were defined as ρ_L = 998.2 kg/m^3 and $\mu_L = 1.003 \times 10^{-3}$ Pa s. The outlet pressure was kept constant and equal to one atmosphere (101 kPa).

Figure 2 illustrates a slug unit cell with length $L = L_s + L_f$ where L_s and L_f are the lengths of the liquid slug and liquid film regions. The slug nose moves with velocity U_T while its tail (or bubble nose) is displaced with velocity U_B. The mixture velocity is U_M, which is equal to the sum of the gas and liquid superficial velocities ($U_M = U_{sG} + U_{sL}$).

Three cases were selected to be presented corresponding to different liquid superficial velocities, while the gas superficial velocity was kept constant (U_{SG} = 0.788 m/s). Case 1: U_{sL} = 0.295 m/s, Case 2: U_{sL} = 0.393 m/s and Case 3: U_{sL} = 0.516 m/s. These cases can be classified as intermittent slug (or elongated bubble) based on classical flow maps (e.g., Mandhane et al., 1974).

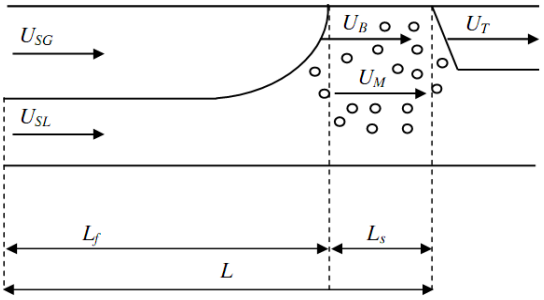

Figure 2. Slug unit cell.

All the results obtained here were determined by imposing a stratified flow as initial condition. However, since only the statistically steady state regime is analyzed, the initial condition does not influence the results.

The instantaneous liquid phase velocities were measured with the optical techniques described, while statistical variables were determined with the photogate cells installed at known positions (Fonseca Jr. et al., 2009). The desired statistical variables were measured with a procedure similar to the one employed in the numerical predictions. The mean experimental uncertainties of the bubble and slug velocities were inferior to 5.6% and 4.4%, respectively, while the slug length uncertainty was inferior to 2.1%.

The slug parameters (length, velocity and frequency) were numerically determined at several fixed positions along the pipe and are compared with the experimentally measured values. Mean values along the pipe are also presented.

Bubble shape and instantaneous velocity field

Figure 3(a) presents the bubble contour recorded for the conditions of Case 3. The images obtained from the several cases (Fonseca Jr. et al., 2009) confirm the findings reported in the literature (Bendiksen, 1984; Rosa and Fagundes Netto, 2004), which indicates that the bubble tip tends to move towards the pipe centerline as the mixture velocity increases. This behavior is believed to be a consequence of the flow separation at the leading bubble tail that displaces the maximum fluid velocity in the liquid slug towards the top of the pipe, downstream of the separated region. The momentum flux displaced to the upper part of the pipe produces a force on the trailing bubble that tends to move its nose toward the pipe centerline, as confirmed by the pictures of Fig. 3.

Figure 3(b) illustrates the instantaneous velocity field obtained by the optical techniques implemented, focusing on a region around the bubble nose for Case 3. It can be noticed the tendency of the flow ahead of the bubble nose assuming a flat profile in most of the pipe cross section, as indicated by the large darker region which is associated with a constant value of the velocity magnitude. It can also be seen a downward flow acting on the bubble nose responsible for its motion toward the pipe centerline. This and other features of the instantaneous velocity field can be observed in Fonseca Jr. et al. (2009).

The focus of the present work will not be on the instantaneous velocity field, but in the statistical properties of the flow. Since a numerical one-dimensional modeling was implemented, velocity field results are not available in the numerical predictions, and comparison cannot be performed.

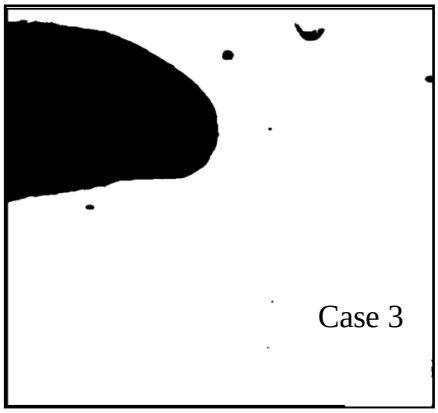

(a) Bubble nose shape.

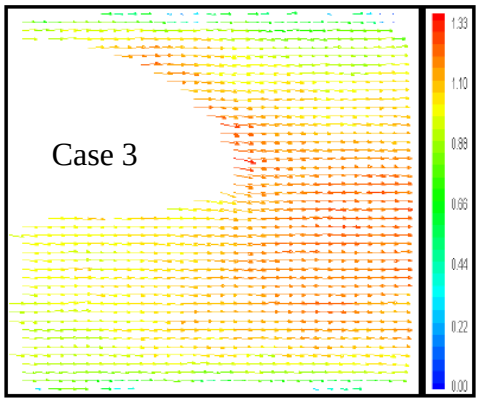

(b) Instantaneous velocity field.

Figure 3. Typical optical results. Case 3: U_{sL} = 0.516 m/s.

Void fraction

The numerically determined time-averaged void fractions near the end of the pipe (x = 9 m) are presented in Table 2, for the three cases studied. Since no experimental data of void fraction was obtained, the numerical results are compared with Rouhani-Axelsson void fraction correlation for horizontal flow (Thome, 2005).

$$\langle \alpha_G \rangle = \frac{\chi / \rho_G}{[\Theta_1 + \Theta_2]} \quad ; \quad \chi = \frac{\rho_G U_{sG}}{(\rho_G U_{sG} + \rho_L U_{sL})} \tag{16}$$

$$\Theta_1 = [1 + 0.12(1-\chi)]\left[\frac{\chi}{\rho_G} + \frac{1-\chi}{\rho_L}\right] \tag{17}$$

$$\Theta_2 = \left[\frac{[1.18(1-\chi)][g\,\sigma(\rho_L - \rho_G)]^{0.25}}{(\rho_G U_{sG} + \rho_L U_{sL})\,\rho_L^{0.5}}\right] \tag{18}$$

Table 2 shows that a reasonable agreement was obtained between the predicted average void fraction values and correlation results, especially for Cases 1 and 2. It can also be seen that the void fraction reduces as the mixture velocity increases, resulting in a larger difference between the results. The discrepancy might be a consequence of the model neglecting the gas entrainment process into the slug body. This will be the subject of future investigation.

Table 2. Mean void fraction.

Cases	U_M (m/s)	α_G numerical	α_G (Steiner, 1993)	Error %
1	1.083	0.678	0.650	4.4
2	1.181	0.643	0.596	8.0
3	1.304	0.549	0.428	28

Slug frequency

Figure 4 is presented to indicate that a statistically steady state regime has been reached. It is a plot of the reciprocal of the time interval between slugs calculated at a fixed axial position, x = 9 m, for Case 2. The time average of this signal is the average slug frequency.

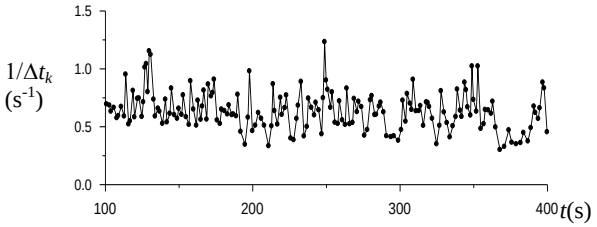

Figure 4. Frequency with time at x = 9 m. Case 2: U_{sL} = 0.393 m/s.

The mean slug frequency obtained numerically is compared with the experimental data in Table 3. Although Case 2 presented a large difference between the predicted and measured data, good agreement was obtained for Cases 1 and 3.

Table 3. Mean slug frequency.

Cases	U_M (m/s)	υ_s (1/s) experimental	υ_s (1/s) numerical	Error %
1	1.083	0.601	0.556	7.50
2	1.181	0.946	0.740	21.8
3	1.304	1.420	1.233	13.1

Slug length

The evolution of the slug length along the pipe is shown in Fig. 5 for all cases studied. Case 1 shows a fast length growth near the entrance and after a distance equal to 5 m, the slug size tends to stabilize, reaching an approximately constant length equal to L_s/D = 25. The other cases present similar behavior, but the initial growth was smoother. This result shows that the processes of slug growth are mainly at the pipe entrance region.

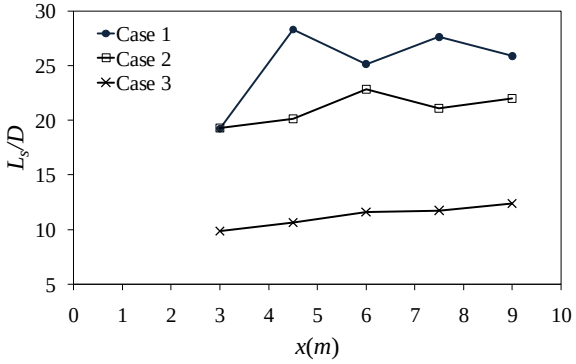

Figure 5. Mean slug length distribution along the channel.

The mean slug lengths determined numerically and measured experimentally are shown in Table 4 for the three cases considered. It can be seen that for all cases, the lengths are within the range from 12 to 26 *D*, agreeing with previously obtained experimental data of different authors: $L_s = 12 - 24D$ (Dukler and Hubbard, 1975), $L_s = 12 - 30D$ (Andreussi and Bendiksen, 1989) and $L_s = 10 - 34D$ (He, 2002).

Table 4. Mean liquid slug length, L_s/D.

Cases	Experimental (L_s/D)	Numerical (L_s/D)
1	19.4	25.3
2	16.2	21.1
3	15.7	11.2

Figures 6 to 8 show the experimental and numerical liquid mean slug length histograms for the three cases, while Figures 9 to 11 correspond to the mean bubble length. The graphs present the ratio of the number of slugs with a certain length by the total number of slugs identified during the data acquisition period. The results correspond to the axial coordinate equal to 9 m, since only at this location the experimental data were measured.

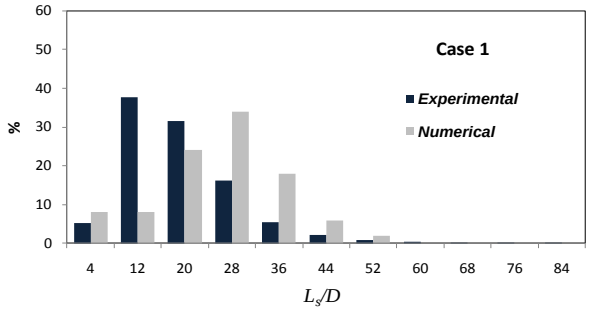

Figure 6. Mean slug length distribution. Case 1: U_{sL} = 0.295 m/s.

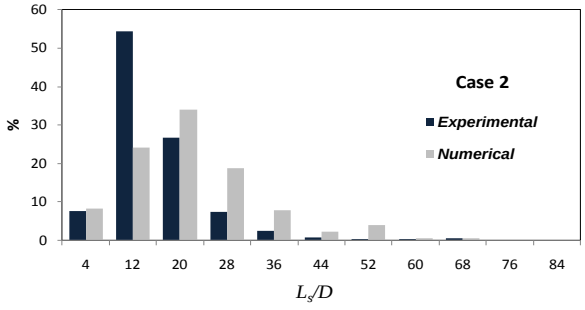

Figure 7. Mean slug length distribution. Case 2: U_{sL} = 0.393 m/s.

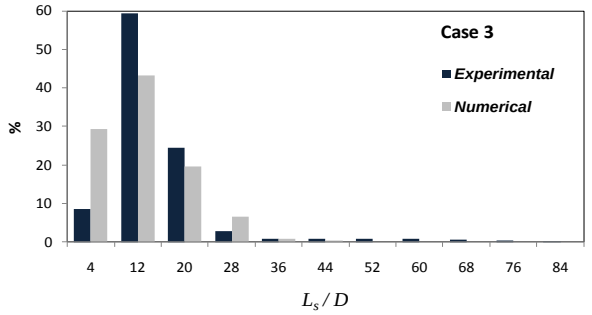

Figure 8. Mean slug length distribution. Case 3: U_{sL} = 0.516 m/s.

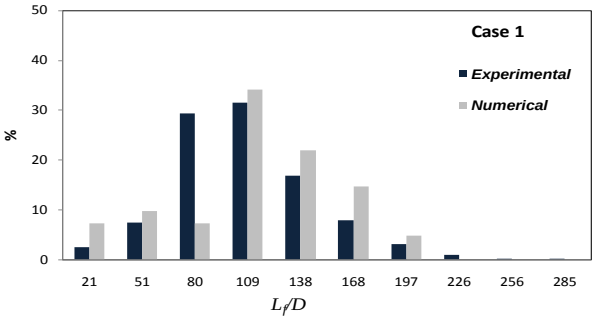

Figure 9. Mean bubble length distribution. Case 1: U_{sL} = 0.295 m/s.

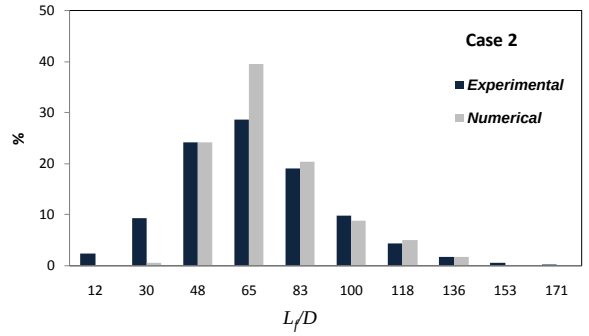

Figure 10. Mean bubble length distribution. Case 2: U_{sL} = 0.393 m/s.

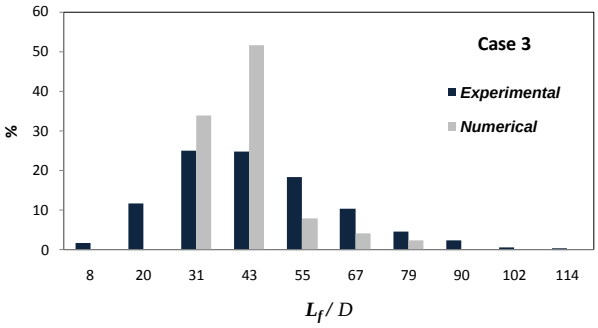

Figure 11. Mean bubble length distribution. Case 3: U_{sL} = 0.516 m/s.

By analyzing the figures, it can be clearly seen the random flow behavior, with a large range of lengths, agreeing with the literature (Fabre and Liné, 1992). A reasonable agreement between the experimental and numerical results for the slug length distribution was obtained, although numerically, a larger range of lengths was predicted. A much better agreement was observed for the bubble length distribution. It can also be noted that when the liquid

superficial velocity increases, the slug frequency increases (Table 4) and the slug length decreases, while the bubble length increases.

Translational slug velocity

Nicklin et al. (1962) presented the following correlation to estimate the translational bubble velocity (or liquid slug tail velocity):

$$U_T = C_o U_M + U_d \tag{19}$$

where U_d is the drift velocity and U_M is the mixture velocity ($U_M = U_{sG} + U_{sL}$). Bendiksen (1984) has experimentally determined the distribution factor C_0 and the drift velocity U_d as a function of the Froude number $Fr_M = U_M/(g\,D)^{0.5}$, based on several flow rates as:

$$Fr_M > Fr_{crit} = 3.5 \;\Rightarrow\; C_o = 1.20, \quad U_d = 0.54\sqrt{gD}$$

$$Fr_M \le Fr_{crit} = 3.5 \;\Rightarrow\; C_o = 1.05, \quad U_d = 0.54\sqrt{gD} \tag{20}$$

The Froude number compares gravitational and inertial forces; therefore, it is widely used in horizontal flows to characterize the degree of stratification of two-phase flows.

For the three cases investigated, the Froude number based on the mixture velocity is within the range [2.32 – 2.69], thus, the distribution factor C_o is 1.05. The mean slug translational velocity determined numerically is compared with Bendiksen correlation (1984) in Table 5. It can be seen that the numerically determined value for C_o agrees with Bendiksen correlation within 12.5%.

Table 5. Distribution parameter C_o.

Cases	U_M (m/s)	C_o Bendiken (1984)	C_o numerical	Error %
1	1.083	1.05	0.987	6.0
2	1.181	1.05	0.919	12.5
3	1.304	1.05	0.964	8.2

Figures 12-14 illustrate the behavior of the mean nose and tail slug velocities along the pipe for all cases. It can be seen that when a slug is formed, the nose velocity is larger than the tail velocity. After the initial acceleration, both velocities diminish along the pipe, until they stabilize at approximately constant values close to the one predicted by Bendiksen's correlation (1984). As expected, this happens at the same position as the slug length reaches an approximate stable length. Since near the entrance of the pipe the slug nose velocity is larger than the tail velocity, slug coalescence occurs, increasing their length, as observed in Fig. 5.

Figure 15 compares the translational slug velocity obtained numerically with Bendiksen's correlation (1984) as a function of the mixture velocity for six cases. A good agreement, with differences less than 10%, was obtained for all mixture velocities.

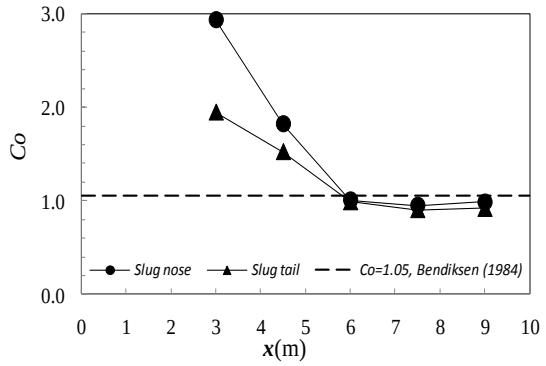

Figure 12. Mean slug nose and tail velocities. Case 1: U_{sL} = 0.295 m/s.

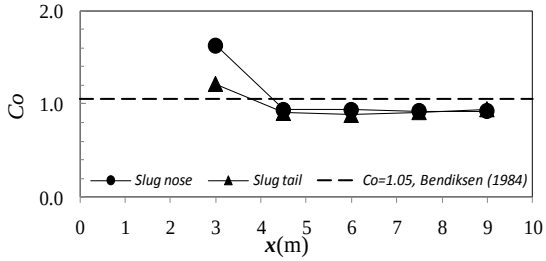

Figure 13. Mean slug nose and tail velocities. Case 2: U_{sL} = 0.393 m/s.

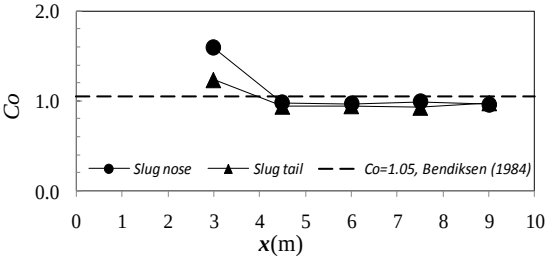

Figure 14. Mean slug nose and tail velocities. Case 3: U_{sL} = 0.516 m/s.

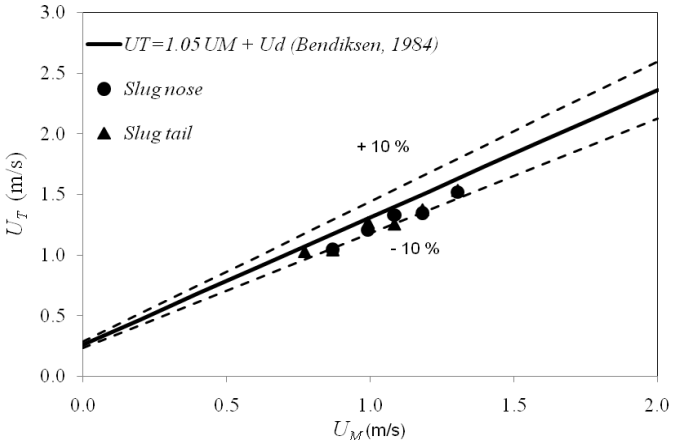

Figure 15. Slug translational velocity versus mixture velocity.

Table 6 presents a comparison of the slug translational velocity measured experimentally and predicted numerically. An excellent agreement was obtained, with differences inferior to 1%. The level of agreement is seen to improve with the increase of the mixture velocity.

Table 6. Mean liquid slug velocity.

Cases	U_M	U_T(m/s)	U_T(m/s)	Error

	(m/s)	experimental	numerical	%
1	1.083	1.32	1.331	0.83
2	1.181	1.35	1.347	0.22
3	1.304	1.52	1.518	0.13

Conclusions

Slug flow of water and air in horizontal pipes was experimentally and numerically investigated. A one-dimensional version of the two-fluid model was implemented. Statistical information on flow parameters like frequency, velocity and slug length was numerically predicted. Statistical information on the slug flow was experimentally determined employing photocells installed in a specially built test section formed by a 400-diameter-length transparent pipe. A combination of three optical techniques was employed to allow the instantaneous measurement of the liquid velocity field and bubble shape. Differences between measured and predicted values varied from 10% to 20% for frequency and slug length, and for the slug translation velocity it was inferior to 1%. Therefore, it can be said that good agreement was verified for the statistical data obtained from experiments and those predicted by Two-Fluid Model implemented.

Acknowledgement

The authors acknowledge the support awarded by PETROBRAS and CNPq – the Brazilian National Council for Scientific and Technological Development.

References

Al Safran, E., Sarica, C., Zhang, H.-Q., Brill, J.P., 2005, "Investigation of Slug Flow Characteristics in the Valley of a Hilly Terrain Pipeline", *Int. J. Multiphase Flow*, Vol. 31, No. 3, pp. 337-357.

Andreussi, P. and Bendiksen, K., 1989, "An Investigation of Void Fraction in Liquid Slugs For Horizontal and Inclined Gas-Liquid Pipe Flow", *Int. J. Multiphase Flow*, Vol. 15, No. 6, pp. 937-46.

Barnea, D. and Taitel, Y., 1993, "A Model for Slug Length Distribution in Gas–Liquid Slug Flow", *Int. J. Multiphase Flow*, Vol. 19, pp. 829-838.

Bendiksen, K.H., 1984, "An Experimental Investigation of the Motion of long bubbles in inclined pipes", *Int. J. Multiphase Flow*, Vol. 10, No. 4, pp. 467-83.

Carneiro, J.N.E.; Ortega, A.J., Nieckele, A.O., 2005, "Influence of the Interfacial Pressure Jump Condition on the Simulation of Horizontal Two-Phase Slug Flows Using the Two-Fluid Model", Proceedings of Computational Methods in Multiphase Flow III, Vol. 1, Portland, Maine, EUA, pp. 123-134.

Carneiro, J.N.E. and Nieckele, A.O., 2008, "Influence of the Interfacial Pressure Jump on Slug Flow Evolution Along Horizontal Pipelines Using the Two-Fluid Model", Proceedings EBECEM 2008 – 1st Brazilian Meeting of Boling, Condensation and Multiphase Liquid-Gas Flow, Florianopolis, SC, Brazil.

Cook, M. and Behnia, M., 2000, "Slug Length Prediction in Near Horizontal Gas-Liquid Intermittent Flow", *Chem. Eng. Sci*., Vol. 55, pp. 2009-2018.

Dukler, A.E. and Hubbard, M.G., 1975, "A Model for Gas-Liquid Slug Flow in Horizontal and Near Horizontal Tubes", *Ind. Eng. Chem. Fundam.*, Vol. 14, pp. 337-345.

Fabre, J. Liné, A., 1992, "Modeling of Two-Phase Slug Flow", Ann. Rev. Fluid Mech., Vol. 24, pp. 21-46.

Fonseca Jr, R., Barras Jr., J.M., Azevedo, L.F.A., 2009, "Liquid Velocity Field and Bubble Shape Measurements in Two-Phase, Horizontal Slug Flow", Proceedings of COBEM 2009, Gramado, RS Brazil, COB09-245.

He, L.M., 2002, "An Investigation of the Characteristics of Oil-Gas Two-Phase Slug Flow in Horizontal Pipes, Ph.D. Thesis, Xi'an Jiaotong University.

Ishii, M., Hibiki, T. 2006, "Thermo-fluid Dynamics of Two-phase Flow", Springer-Verlag.

Issa R.I. and Kempf, M.H.W., 2003, "Simulation of Slug Flow in Horizontal and Nearly Horizontal Pipes with the Two–Fluid Model", *Int. J. of Multiphase Flow*, Vol. 29, pp. 69-95.

Kvernvold, O., Vindoy, V., Sontvedt, T., Saasen A. and Selmer-Olsen S., 1984, "Velocity Distribution in Horizontal Slug Flow", *Int. J. Multiphase Flow*, Vol. 10, No. 4, pp. 441-457.

Mandhane, J.M., Gregory, G.A., Aziz, K., 1974, "A Flow Pattern Map for Gas-Liquid Flow in Horizontal Pipes", *Int. J. Multiphase Flow*, Vol. 1, pp. 537-53.

Nicklin, D., Wilkes, J., Davidson, J., 1962, "Two-Phase Flow in Vertical Tubes", *Trans. Inst. Chem. Engrs.*, Vol. 40, pp. 61-68.

Ortega, A.J. and Nieckele, A.O., 2005, "Simulation of Horizontal Two-Phase Slug Flows Using the Two-Fluid Model with a Conservative and Non-Conservative Formulation", Proceedings of COBEM 2005, Ouro Preto, MG, Brazil, COB05-0153.

Raffel, M., Willert, C., Kompenhans, J. and Wereley, S., "Particle Image Velocimetry: a practical guide", Springer, 2007.

Rosa, E.S., Fagundes Netto, J.R.., 2004, "Viscosity Effect and Flow Development in Horizontal Slug Flows", 5th Int. Conf. on Multiphase Flow, ICMF" 04 Yokohama, Japan, Paper No. 306, 2004.

Sanchis, A., Johnson, G.W., Jensen, A., 2011, "The Formation of Hydrodynamic Slugs by The Interaction of Waves In Gas-Liquid Two-Phase Pipe Flow", *Int. J. Multiphase Flow*, Vol. 37, No. 4, pp. 358-368.

Sharma, S., Lewis, S., Kojasoy, G., 1998, "Local Studies in Horizontal Gas-Liquid Slug Flow", *Nuclear Engineering and Design*, Vol. 184, pp. 305-318.

Thome, J.R., 2005, "Condensation in Plain Horizontal Tubes: Recent Advances in Modelling of Heat Transfer to Pure Fluids and Mixtures", *J. of the Braz. Soc. of Mech. Sci. & Eng.*, Vol. 27, No. 1, pp. 23-30.

Taitel, Y. and Dukler, A.E., 1976, "A Model for Predicting Flow Regime Transitions in Horizontal and Near Horizontal Pipes", *AIChE J.*, Vol. 22, pp. 47-55.

Want, X., Guo, L., Zhang, X., 2007, "An Experimental Study of the Statistical Parameters of Gas-Liquid Two-Phase Slug Flow in Horizontal Pipeline", *Int. J. Heat Mass Transfer*, Vol. 50, pp. 2439-2443.

Woods, B.D., Fan, Z., Hanratty, T.J., 2006, "Frequency and Development of Slugs in a Horizontal Pipe at Large Liquid Flow", *Int. J. Multiphase Flow*, Vol. 32, pp. 902-925.